THE JOURNAL OF PHYSICAL CHEMISTRY B

Article

pubs.acs.org/JPCB

# Ligand 5,10,15,20-Tetra(*N*-methyl-4-pyridyl)porphine (TMPyP4) Prefers the Parallel Propeller-Type Human Telomeric G-Quadruplex DNA over Its Other Polymorphs

Asfa Ali,[†] Manju Bansal,[§] and Santanu Bhattacharya*[,†,‡]

[†]Department of Organic Chemistry, Indian Institute of Science, Bangalore 560 012, India

[‡]Jawaharlal Nehru Centre for Advanced Scientific Research, Bangalore 560 064, India

[§]Molecular Biophysics Unit, Indian Institute of Science, Bangalore 560 012, India

Supporting Information

**ABSTRACT:** The binding of ligand 5,10,15,20-tetra(*N*-methyl-4-pyridyl)-porphine (TMPyP4) with telomeric and genomic G-quadruplex DNA has been extensively studied. However, a comparative study of interactions of TMPyP4 with different conformations of human telomeric G-quadruplex DNA, namely, parallel propeller-type (PP), antiparallel basket-type (AB), and mixed hybrid-type (MH) G-quadruplex DNA, has not been done. We considered all the possible binding sites in each of the G-quadruplex DNA structures and docked TMPyP4 to each one of them. The resultant most potent sites for binding were analyzed from the mean binding free energy of the complexes. Molecular dynamics simulations were then carried out, and analysis of the binding free energy of the TMPyP4−G-quadruplex complex showed that the binding of TMPyP4 with parallel propeller-type G-quadruplex DNA is preferred over the other two G-quadruplex DNA conformations. The results obtained from the change in solvent excluded surface area (SESA) and solvent accessible surface area (SASA) also support the more pronounced binding of the ligand with the parallel propeller-type G-quadruplex DNA.

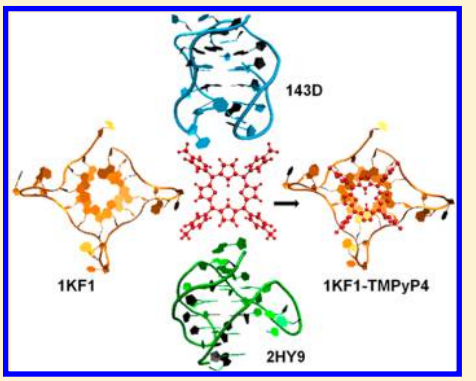


## INTRODUCTION

In eukaryotes, the telomeric ends of the chromosomes comprise tandem repeats of sequences enriched in guanine bases such as $d(T_2AG_3)$ in humans, $d(G_4T_2)$ in *Tetrahymena*,[1] and $d(G_4T_4)$ in *Oxytricha*.[2] These telomeres play a vital role in the cell aging (senescence) and death.[3,4] In human somatic cells, the telomeric DNA extends over a stretch of 5−8 kilobases of which nearly 100−200 bases protrude as a 3′-single-stranded overhang.[5] Unlike in normal cells where 50−200 bases are lost during the process of replication, in cancer cells this shortening is inhibited due to the activation of an enzyme called telomerase.[6] This enzyme is statistically found to be activated in almost 85% of the human cancer cells.[7] Researchers are doing their utmost to stop the proliferation of cancer cells by stabilizing the G-quadruplex structures in the telomeric ends, thereby suppressing the action of telomerase.[8,9] These G-quadruplex secondary structures, composed of a stacked array of G-quartets,[10,11] are therefore targeted as putative binding sites for anticancer agents.[12,13] Consequently, the design of organic small molecules (ligands) is being carried out to achieve stabilization of these guanine-rich scaffolds.[14−17]

Apart from the telomeric ends of the chromosomes, the G-quadruplex DNA structures also exist in various genomic regions such as fragile X-syndrome triplet repeats,[18,19] the regulatory region of insulin gene,[20] the dimerization region of HIV,[21] and in the promoter sequences like c-*myc* gene, etc.[22] Various ligands interacting with the G-quadruplex DNA such as amidoanthraquinones,[23] oxazoles,[24] fluorenones,[25] perylenes,[26,27] acridines,[28,29] benzimidazoles,[30−35] etc., are known, and many of them have the potential to become antitumor agents by acting as telomerase inhibitors. Porphyrins belong to a class of drugs that have been studied extensively and are known for their excellent affinity toward the G-quadruplex DNA structures.[36−43] A comparison of the three positional isomers of the cationic porphyrins, namely, 5,10,15,20-tetra(*N*-methyl-2-pyridyl)porphine (TMPyP2), 5,10,15,20-tetra(*N*-methyl-3-pyridyl)porphine (TMPyP3), and 5,10,15,20-tetra-(*N*-methyl-4-pyridyl)porphine (TMPyP4) (Figure 1), toward the stabilization of the G-quadruplex DNA structures has been reported using the gel mobility shift and helicase assay experiments.[44] Earlier studies have also shown that tetrakis(4-*N*-methylpyridyl)porphine ($H_2$TMPyP) intercalates with the duplex DNA.[45] Hurley and co-workers have demonstrated that, in the case of G-quadruplex DNA, TMPyP4 stacks externally on the G-quartets of the human telomeric DNA sequences and no intercalation occurs.[46] This is supported by UV and one-dimensional high field NMR experiments on a variety of G-rich

**Received:** June 11, 2014
**Revised:** December 3, 2014

   dx.doi.org/10.1021/jp505792z | *J. Phys. Chem. B* XXXX, XXX, XXX−XXX

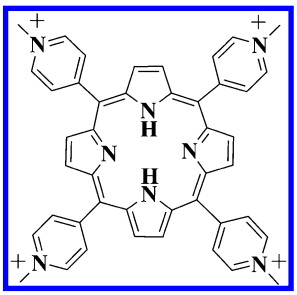

**Figure 1.** Molecular structure of the ligand, 5,10,15,20-tetra(*N*-methyl-4-pyridyl)porphine (TMPyP4).

DNA sequences, forming parallel-stranded G-quadruplexes like $d(T_2AG_3)$, $d(T_2AG_3T_2)$, and $d(T_2AG_3T_2A)$.[46]

Our principal focus in the present work is to study the interaction of TMPyP4 with different 22-mer human telomeric G-quadruplex DNA morphologies. Though various studies have been reported earlier about the binding affinity of porphyrin ligand toward various G-quadruplex forming sequences either in the telomeric regions or in the oncogenes, there is lack of information about the exact nature of interaction with various G-quadruplex DNA secondary structures. Besides stacking at the ends of the G-tetrads, the ligands, in general, also have an affinity toward the loop regions and the grooves of the G-quadruplex. Accordingly, our primary attempt has been to find the appropriate site of binding of TMPyP4 in the entire G-quadruplex DNA structure, using an extensive docking procedure where the search algorithm was first applied to the total macromolecule ("blind" docking) followed by selective docking at all the possible binding sites. The docked complex was then subjected to molecular dynamics (MD) simulations keeping the conditions close to the cellular environment. This yielded a putative picture of the precise fit of porphyrin ligands into the loops, into the grooves, or over the surface of the G-tetrads. From this, quantitative information is obtained about the binding affinity of TMPyP4 toward the G-quadruplex DNA structures.

## METHODOLOGY

For the molecular modeling studies, we focused on the 22-mer human telomeric G-quadruplex DNA, 5′-AGGGTTAGGGTT-AGGGTTAGGG-3′, having three different morphologies whose coordinates have been extracted from the Protein Data Bank. We considered the X-ray crystal structure of parallel propeller-type with PDB ID 1KF1[47] (PP), the NMR based solution structure of antiparallel basket-type having PDB ID 143D[48] (AB), and the NMR structure of mixed hybrid-type with PDB ID 2HY9[49] (MH) G-quadruplex DNA for our study (Figure 2).

The structure of TMPyP4 was obtained using the software GaussView 3.09 and was optimized at the B3LYP level of theory with 6-31G* as the basis set using *Gaussian 03*.[50] The Mülliken atomic charges of the optimized ligand obtained from the calculation at the B3LYP/6-31G* level of theory were used for the docking studies. AM1-BCC was employed as the charge method for the calculation of partial charges in the *antechamber* module of *Amber 9* software.[51] In conjunction with the *antechamber* program, GAFF (general AMBER force field)[52] was used to create files of porphyrin so that it can be recognized by *leap*. Also, the missing parameters of the ligand were taken care of by *parmchk* which generated other required parameters.

**Docking.** In order to find out the exact binding mode of TMPyP4 to the above-mentioned G-quadruplex sequences, we used the optimized structure of TMPyP4 and allowed it to dock to three G-quadruplex DNA structures, namely, the parallel propeller-type (PP), the antiparallel basket-type (AB), and the mixed hybrid-type (MH) using *AutoDock 4.0* which uses the free energy of binding as the basis for its empirical scoring function.[53,54] The polar and aromatic hydrogens were added to each DNA by *AutoDockTools* (ADT).[55] We used the Lamarckian Genetic Algorithm which is one of the widely used stochastic search algorithms which unites the properties of both the local search algorithm (Solis and Wets algorithm)[56] and the global search algorithm (genetic algorithm).

A "blind" docking of TMPyP4 was carried out with the three G-quadruplex DNAs in which the grid box dimensions were selected such that it encompassed each of the entire DNA molecules. The resolution was set to 0.375 Å, and after adjusting the grid box to the center of the macromolecule, the *AutoGrid* maps were created for every atom type in TMPyP4 along with the electrostatics map and a desolvation map.

Initially, each docking operation comprised 150 runs with an initial population of 150 individuals with a maximum number of 27 000 generations and the maximum number of energy evaluations was set to 2 500 000. We allowed crossover and mutation to take place at a rate of 0.8 and 0.02, respectively. Results which occurred within a root-mean-square deviation (RMSD) of 2.0 Å were grouped in the same cluster. However, as we considered the entire macromolecule in the grid box, we did not use RMSD as a measure of accuracy in the "blind" docking; instead, we opted to classify the modes of binding as end-stacking, groove binding, and others.

A second series of docking (selective docking) was performed where smaller grid boxes were generated around the potential binding sites and TMPyP4 was allowed to dock to these sites separately. On the basis of the RMSD accuracy criterion, we calculated the clustering histogram of the docking runs to the three different G-quadruplex DNAs. Finally, on the basis of binding affinity value and clustering pattern, we

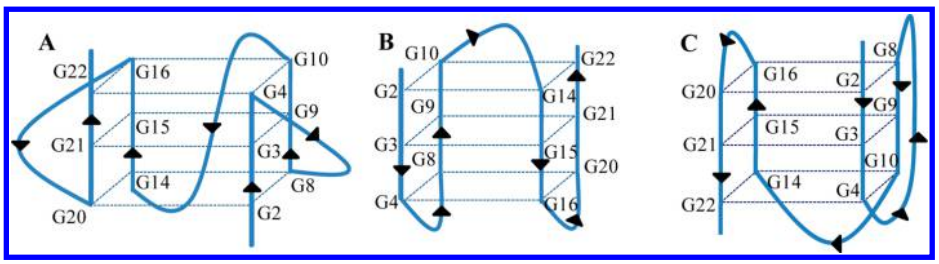


**Figure 2.** Schematic representation of human telomeric 22-mer G-quadruplex DNA morphologies: (A) parallel propeller-type (PP), (B) antiparallel basket-type (AB), and (C) mixed hybrid-type quadruplex (MH).


dx.doi.org/10.1021/jp505792z | *J. Phys. Chem. B* XXXX, XXX, XXX–XXX

selected the most stable docked conformer in each case. Thus, we generated the three most stable structures which represented the most potent complexes formed by the porphyrin ligand and each of the three G-quadruplex DNAs.

**Molecular Dynamics Simulation.** The three association complexes obtained from the docking studies were considered as the starting structures for the respective molecular dynamics simulation studies. However, we also performed a MD simulation of native DNA keeping the same protocol in order to understand the changes that occur upon the binding of porphyrin with the G-quadruplex DNA. All the simulation studies were carried out using the *Amber 9* software package along with *AmberTools 1.3*. To the initial structure of the G-quadruplex DNA, hydrogen atoms were added at the predetermined positions by the *tleap* module of *Amber 9*. $K^+$ ions were added at the regions of high negative electrostatic potentials around the DNA in order to neutralize it.[57] The system was then solvated explicitly[58] using a 10 Å truncated octahedral shell of pre-equilibrated TIP3P water. The simulations were carried out using the *sander* module of *Amber 9* and the force field ff99bsc0[59−64] obtained from *AmberTools 1.3*. The bonds involving hydrogen were constrained by using the SHAKE algorithm, and the temperature of the system was regulated by the Langevin temperature equilibration scheme. Furthermore, we used periodic boundary conditions based on the particle mesh Ewald (PME) method whereby the long-range electrostatics was taken into consideration. The root-mean-square deviation (RMSD) values were calculated by *ptraj*, and the results were analyzed using Pymol[65] and VMD.[66]

**Minimization.** As observed in the crystal structure of the 22-mer G-quadruplex DNA structures,[47] the presence of the central $K^+$ ions is essential for the stability of the G-quadruplex DNA morphology. Hence, the two central $K^+$ ions were placed manually between the G-tetrads before the simulation studies. All the G-quadruplex DNAs and the G-quadruplex−porphyrin complexes were allowed to undergo two stages of energy minimizations. The first stage of minimization involved the use of positional restraints in order to keep the G-quadruplexes and the two central $K^+$ ions rigid with force constants of 500 and 50 kcal $mol^{-1}$, respectively. We performed 1000 steps of minimization where the initial 500 steps were minimized using the steepest descent method and the remaining using the conjugate gradient method. The cutoff value for the long-range nonbonded interaction was assigned to be 10 Å. After minimization of the water and bulk $K^+$ ions, we minimized the whole system without restraints for 2500 steps.

**Dynamics.** The minimized structures were subjected to an equilibration protocol in which the system was heated from 0 to 300 K for 20 ps at constant volume with restraints of 50 kcal $mol^{-1}$ for the DNA and central $K^+$ ions. Langevin dynamics has been applied to control the temperature using a collision frequency of 1.0 $ps^{-1}$, and the molecular dynamics is run with a time step of 2 fs per step. After successfully heating the system at constant volume, the system was switched on to constant pressure. The system was then allowed to equilibrate with gradually reducing constraints (50, 40, 30, 20, 10 kcal $mol^{-1}$) for 50 ps each at a temperature of 300 K. A final 1 ns equilibration run was performed to provide our system ample time to relax with a minimal restraint of only 5 kcal $mol^{-1}$ followed by a 50 ns production run devoid of any restraints. A constant pressure periodic boundary condition was applied with an average pressure of 1 atm, and the pressure was maintained by isotropic position scaling with a relaxation time of 2 ps.

**Free Energy Calculations.** In order to calculate the free energy difference between the TMPyP4 bound state and the unbound state of G-quadruplex DNA, we used the MM_PBSA [molecular mechanics (MM), Poisson−Boltzmann (PB), surface area] module of *Amber 9*. The electrostatic contribution to the solvation free energy was calculated with the *pbsa*[67] program which utilizes the Poisson−Boltzmann (PB) method and also by the generalized Born (GB) method as implemented in the *sander* module of *Amber 9*. MM_PBSA calculations were performed on the last 10 ns of the final production run of each of the TMPyP4−G-quadruplex complexes. In order to obtain a set of representative structures, we collected snapshots for each complex in addition to the snapshots for the G-quadruplex alone and TMPyP4 which were extracted from the complex trajectory after equilibration.

For the MM_PBSA calculation, all the water molecules and $K^+$ ions were eliminated from the snapshots, except for the two $K^+$ ions placed in the central core of the G-quartets. The radius of the $K^+$ ion was set to 1.33 Å.[68] A total of 100 snapshots were extracted for the last 10 ns using the single trajectory approach. The independent free energies of the G-quadruplex DNA, TMPyP4, and the TMPyP4−G-quadruplex complex were estimated. MM_PBSA calculates the binding free energy for the interaction of TMPyP4 with various 22-mer G-quadruplex DNAs according to eq 1.

$$\Delta G = G(\text{complex}) - G(G\text{-quadruplex DNA}) - G(\text{TMPyP4}) \quad (1)$$

The dielectric constant values were set to 1 and 80 for the solute and surrounding solvent, respectively. The solvent probe radius was assigned a default value of 1.4 Å. 1000 iterations were performed with the linear PB equation where a lattice spacing of two grids was maintained per angstrom. The nonpolar contribution to desolvation was calculated by *molsurf*[69] inherently built in the MM_PBSA module used. The solvent accessible surface area (SASA) was used to derive the nonpolar free energy ($\Delta G_{NP}$) as per eq 2.

$$\Delta G_{NP} = \gamma \text{SASA} + b \quad (2)$$

where $\gamma$ = 0.0072 kcal/(mol·Å$^2$) and $b$ = 0.00 kcal $mol^{-1}$.

With the assumption that the conformation of the G-quadruplexes remained the same during the MD simulation in the free and TMPyP4 bound state, we can calculate the binding free energy as

$$\Delta E_{GAS} = \Delta E_{ELEC} + \Delta E_{VDW} + \Delta E_{INT}$$

$$\Delta G_{SOL} = \Delta G_{NP} + \Delta G_{PB}$$

$$\Delta G = \Delta E_{GAS} + \Delta G_{SOL} - T\Delta S_{GAS}$$

$$\Delta G \sim (\Delta E_{GAS} + \Delta G_{SOL})$$

where $\Delta E_{GAS}$ is the sum of the electrostatic energy ($\Delta E_{ELEC}$), the van der Waals contribution ($\Delta E_{VDW}$), and the internal energy arising from bond angle and dihedral terms ($\Delta E_{INT}$) in the gaseous phase as calculated from the molecular mechanics force field. While $\Delta G_{NP}$ refers to the nonpolar contribution to the solvation free energy, $\Delta G_{PB}$ refers to the electrostatic contribution as obtained from the PB calculations. The sum of the polar and nonpolar contributions comprises the solvation free energy $\Delta G_{SOL}$. It has been found[70] that the $T\Delta S_{GAS}$ value


dx.doi.org/10.1021/jp505792z | J. Phys. Chem. B XXXX, XXX, XXX−XXX

remains almost constant, thereby not causing any difference in the trend of the free energy data. Thus, the final estimated binding free energy is a summation of the $\Delta E_{GAS}$ and $\Delta G_{SOL}$ terms. The entropic calculations were performed by the normal-mode analysis (nmode module) to obtain the translational, rotational, and vibrational entropy for the receptor, ligand, and complex using the single trajectory approach. A total of 100 snapshots were chosen from the last 10 ns of each trajectory for the nmode analysis. Each snapshot was subjected to minimization followed by the estimation of the entropy. The distance-dependent dielectric constant was set to 1.0 with strict convergence criteria for minimized energy gradient ($10^{-10}$ kcal mol$^{-1}$ Å$^{-1}$). The maximum number of minimization cycles per snapshot in sander was set to $10^{11}$.

**Solvent Accessible Surface Area Calculation.** The solvent accessible surface area was calculated for all the G-quadruplex DNA and their complexes with TMPyP4 with an in-built MSMS module in *AutoDockTools*. MSMS[71] calculates a triangulated surface by translating the PDB atom names into the Connolly numeric codes and atomic radii. The radius of the solvent molecule used as the probe is 1.50 Å.

## RESULTS AND DISCUSSION

**Docking.** Ligand TMPyP4 was docked to each of the G-quadruplex DNA structures by considering the entire macromolecule as its search space. *AutoDock 4.0* efficiently found the most potent binding site in the macromolecule. The results of the "blind" docking of TMPyP4 to PP, AB, and MH (termed as $PP_0$, $AB_0$, and $MH_0$, respectively) are listed in Table S1 (Supporting Information). The lowest binding energy (L.B.E.) and the mean binding energy (M.B.E.) suggest that TMPyP4 binds most efficiently with the parallel propeller-type (PP) G-quadruplex DNA. Although binding of TMPyP4 with MH yields a low binding energy, the clustering pattern indicates a fairly good chance of its binding.

However, in order to avoid missing any of the probable sites, we again performed docking selectively at each of the sites, namely, the end-stacking sites and the grooves of the G-quadruplex DNA. The binding energy of TMPyP4 for docking at all the probable binding sites of each G-quadruplex DNA is summarized in Table 1. The grid box has been selected around the outermost G-tetrad which marks the two end-stacking positions ($X_1$ and $X_2$) for the G-quadruplex X, where X refers to the parallel propeller-type (PP), antiparallel basket-type (AB), and mixed hybrid-type (MH) G-quadruplex DNA. Also, we created a grid box around T5−T6−A7, T11−T12−A13, T17−T18−A19, and the respective tetrads and that due to A1 and the corresponding G-tetrads, so that all the probable groove binding positions ($X_3$−$X_6$) are taken into consideration (Figure S1, Supporting Information). It should, however, be mentioned that in the case of antiparallel basket-type G-quadruplex DNA, selection of search space around one stacking tetrad ($AB_2$) does not result in exact stacking of TMPyP4 to the G-tetrad; instead, it drives itself to the best binding position which is portrayed as a high magnitude of the binding affinity value. Also, in the case of mixed hybrid-type G-quadruplex, selection of one of the end-stacking positions ($MH_1$) leads to a position where it is in association with the two thymines (T11 and T12).

**Table 1. A Comparison of Selective Docking of TMPyP4 with Different G-Quadruplex DNA[a]**

| | | | | | | |
|---|---|---|---|---|---|---|
| complex | $PP_1$ | $PP_2$ | $PP_3$ | $PP_4$ | $PP_5$ | $PP_6$ |
| M.B.E. | −7.86 | −8.38 | −3.26 | −5.24 | −4.18 | −6.05 |
| complex | $AB_1$ | $AB_2$ | $AB_3$ | $AB_4$ | $AB_5$ | $AB_6$ |
| M.B.E. | 14500.0 | −6.28 | −1.63 | −5.50 | −2.17 | −5.95 |
| complex | $MH_1$ | $MH_2$ | $MH_3$ | $MH_4$ | $MH_5$ | $MH_6$ |
| M.B.E. | 1300.0 | 14300.0 | −2.03 | −3.54 | −2.17 | −6.81 |

[a] $PP_1$−$PP_2$, $AB_1$−$AB_2$, $MH_1$−$MH_2$ = end-stacking positions of PP, AB, and MH G-quadruplex DNA, respectively. $PP_3$−$PP_6$, $AB_3$−$AB_6$, $MH_3$−$MH_6$ = groove binding positions of PP, AB, and MH G-quadruplex DNA, respectively. M.B.E. = mean binding energy in kcal mol$^{-1}$.

Different docked positions of TMPyP4 to PP are shown in Figure 3 where it can be clearly seen that the optimum binding has been shown in the case of $PP_2$ with a mean binding energy (M.B.E.) of −8.38 kcal mol$^{-1}$. Likewise, Figures 4 and 5 portray the various binding modes of AB and MH, respectively, with $AB_2$ and $MH_6$ having the highest magnitude of M.B.E. values in the case of the corresponding G-quadruplexes.

By carefully considering all the possibilities of binding of TMPyP4 to different G-quadruplex DNAs under consideration, we sorted out the most stable binding conformation in each case according to their mean binding energy and observed that $PP_2$, $AB_2$, and $MH_6$ are the most stable conformers of the docked complexes. Moreover, the binding sites are independent and nonequivalent.[72] Also, as the binding of one TMPyP4 does not influence the binding of other TMPyP4 molecules (noncooperative binding) to the G-quadruplex DNA,[72] we have considered the best binding site for further simulation.

**MD Simulation Studies.** All the G-quadruplex DNA structures and the corresponding most stable structures of the TMPyP4−G-quadruplex complexes were subjected to MD simulations using the same protocol in all of the cases. Although all the G-quadruplexes are composed of 22-mer human telomeric nucleotide sequences with repeating d-($T_2AG_3$) units, each contains loops with different orientations[73] and inherent groove widths. This disparity becomes the primary driving force for the binding site selectivity of porphyrin toward the various G-quadruplex morphologies.

**Parallel Propeller-Type G-Quadruplex (PP) DNA and Its Complex with TMPyP4 ($PP_2$).** The interaction of TMPyP4 with the parallel propeller-type G-quadruplex DNA was studied. It has three TTA loops and four grooves which have nearly comparable widths (9.0−10.3 Å)[47] along with an almost bare G-tetrad which leads to two optimal end-stacking sites. The final structure of both the native DNA and its complex with TMPyP4 after completion of the final 50 ns production run is shown in Figure 6A and B. The RMSD values for all heavy atoms of the G-quadruplex DNA were found to be ∼2 Å (Figure 6C).

**Antiparallel Basket-Type G-Quadruplex (AB) DNA and Its Complex with TMPyP4 ($AB_2$).** The NMR solution structure of the antiparallel basket-type G-quadruplex DNA exhibits three TTA loops where only two loops participate in forming two prominent grooves and the third diagonally covers one end of the G-tetrad. A molecular dynamics simulation study was performed on the G-quadruplex and complex $AB_2$, and their final structures are shown in Figure 7A and B. The RMSD data show a value of ∼2.5 Å for AB which slightly decreases on complexation ($AB_2$) (Figure 7C).

**Mixed Hybrid-Type G-Quadruplex (MH) DNA and Its Complex with TMPyP4 ($MH_6$).** Like the other two G-quadruplex DNA structures, the hybrid-type mixed parallel−


dx.doi.org/10.1021/jp505792z | J. Phys. Chem. B XXXX, XXX, XXX−XXX

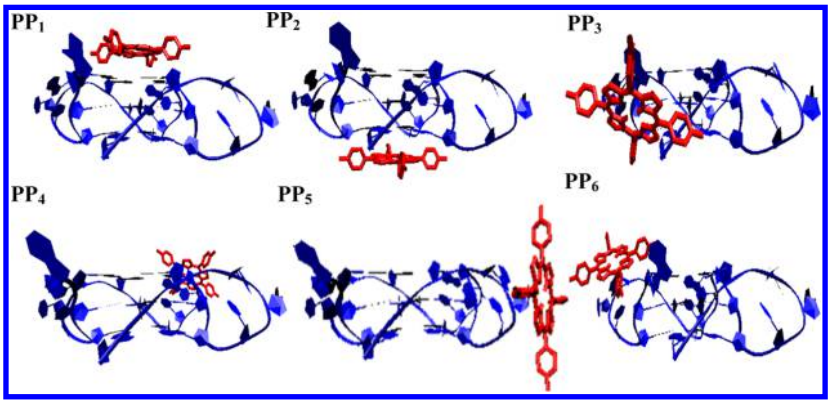


**Figure 3.** Structures of TMPyP4 and the parallel propeller-type native G-quadruplex DNA (PP) are shown in red and blue, respectively. $PP_1$ and $PP_2$ represent the end-stacking sites, and $PP_3$–$PP_6$ represent the four groove binding sites.

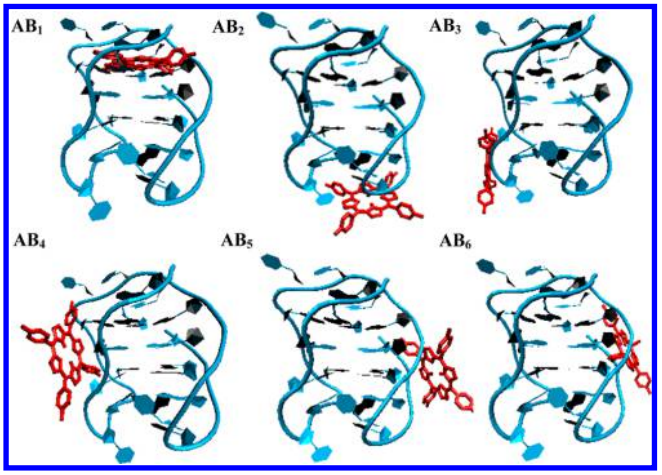


**Figure 4.** Structures of TMPyP4 and the antiparallel basket-type native G-quadruplex DNA (AB) are shown in red and cyan, respectively. $AB_1$ and $AB_2$ represent the end-stacking sites, and $AB_3$–$AB_6$ represent the four groove binding sites.

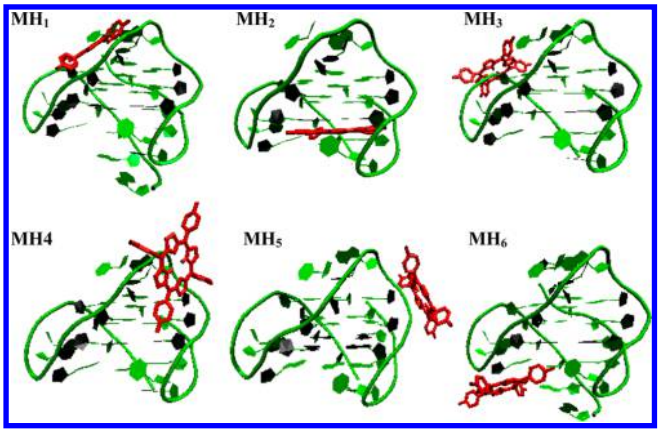


**Figure 5.** Structures of TMPyP4 and the mixed hybrid-type native G-quadruplex DNA (MH) are shown in red and green, respectively. $MH_1$ and $MH_2$ represent the end-stacking sites, and $MH_3$–$MH_6$ represent the four groove binding sites.

antiparallel stranded G-quadruplex DNA also consists of three TTA loops. However, it forms four grooves of unequal widths which comprise one wide groove, two grooves of intermediate width, and one narrow groove.[49] The final structures after the MD simulation along with their RMSD values are shown in Figure 8A and B. After a complete MD simulation run for 50 ns, the RMSD of the G-quadruplex DNA (MH) along with its complex with TMPyP4 ($MH_6$) was calculated. For the native G-quadruplex DNA, the RMSD value was found to be ~3 Å. However, upon complexation, there occurs a steady rise in the RMSD which stabilizes after ~30 ns (Figure 8C).

**Role of Ions.** The presence of metal ions plays a vital role in the stability of the G-tetrads and also in retaining the morphology of the G-quadruplex DNA.[74−77] In fact, the simulation of the same G-quadruplex structures without the two $K^+$ ions in the core of the tetrads using the same protocol in *Amber 9* resulted in a loss of coplanarity of the guanine planes. Also, the RMSD increased to higher values, ranging from ~3.5 to 4.5 Å in the case of the native G-quadruplex DNA and from ~2.8 to 3.5 Å in the case of the TMPyP4–G-quadruplex complex.

In the case of all three native G-quadruplex DNA structures and their corresponding complexes, the two central $K^+$ ions between the G-tetrads were retained, which conforms to the stability of the G-quadruplex DNA structures. Here, $G_I$, $G_{II}$, and $G_{III}$ are assumed to be the three G-tetrads in all of the native G-quadruplex DNA (shown in Figure S1, Supporting Information) and TMPyP4–G-quadruplex complex structures. This is also further supported by the hydrogen bonding data throughout the 50 ns MD simulation runs.

**Hydrogen Bonding Analysis.** The stability of the G-quadruplex DNA is primarily dependent on the stability of the guanine quartets which are linked by the Hoogsteen hydrogen bonds.[78,79] The occupancies of hydrogen bonds for 50 ns MD simulation for all the native G-quadruplex DNAs and their complexes with TMPyP4 are enlisted in Table S2 (Supporting Information) and Table 2, respectively. It is found from Table S2 (Supporting Information) that the Hoogsteen hydrogen bonds, which are essential for the stability of G-tetrads, are retained throughout the entire simulation, thereby verifying the stability of the native G-quadruplex DNA during the simulation.

The analysis of the Hoogsteen hydrogen bond occurrence in the TMPyP4–G-quadruplex complex gives a measure of the stability of the guanine tetrads during the simulation (Table 2). Here, it has been observed that, irrespective of the various conformations of the G-quadruplex DNA structures, the ligand, TMPyP4, stabilizes the structures without causing any major perturbation in the systems throughout the sampling space of 50 ns.

**Solvent Accessible Surface Area.** The solvent accessible surface area (SASA) along with the solvent excluded surface area (SESA) have been calculated using the MSMS module in


dx.doi.org/10.1021/jp505792z | J. Phys. Chem. B XXXX, XXX, XXX–XXX

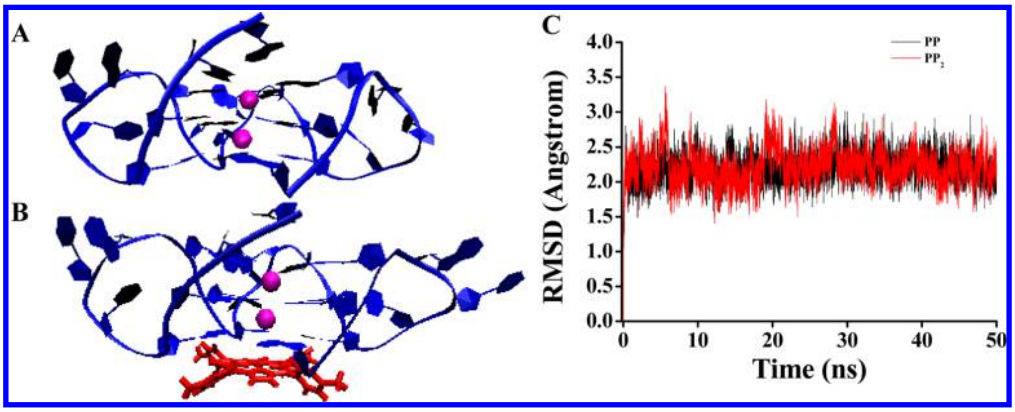


**Figure 6.** Final structures after simulation for 50 ns of (A) native G-quadruplex PP DNA and (B) complex $PP_2$. The structures of TMPyP4, PP DNA, and $K^+$ ions are shown in red, blue, and purple, respectively. Panel C shows the RMSD plots of PP and $PP_2$.

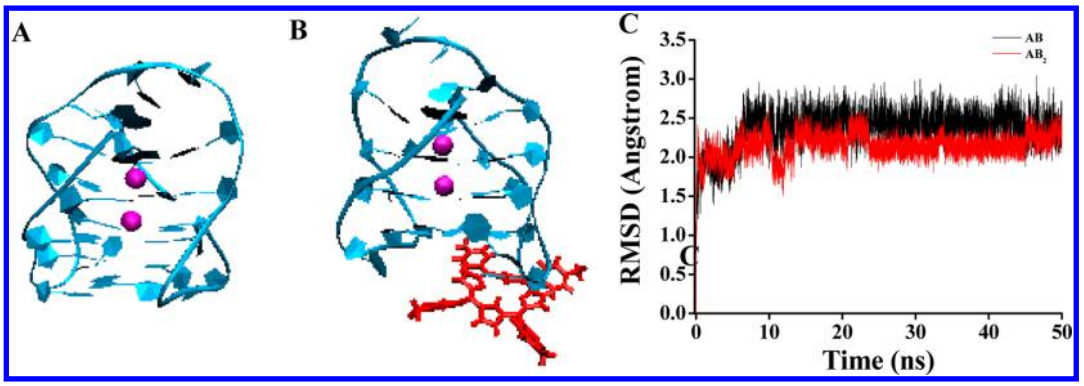


**Figure 7.** Final structures after simulation for 50 ns of (A) native G-quadruplex AB DNA and (B) complex $AB_2$. The structures of TMPyP4, AB DNA, and $K^+$ ions are shown in red, cyan, and purple, respectively. Panel C shows the RMSD plots of AB and $AB_2$.

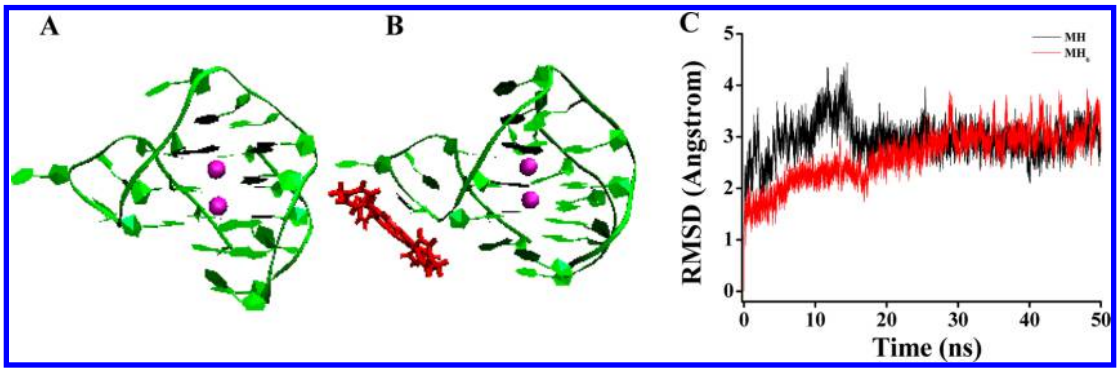


**Figure 8.** Final structures after simulation for 50 ns of (A) native G-quadruplex MH DNA and (B) complex $MH_6$. The structures of TMPyP4, MH DNA, and $K^+$ ions are shown in red, green, and purple, respectively. Panel C shows the RMSD plots of MH and $MH_6$.

*AutoDockTools* (Table 3). It has been observed that there occurs a reduction in both SESA and SASA on complexation of TMPyP4 with the G-quadruplex DNA and this decrease is observed to be maximum in the case of TMPyP4 binding to the tetrad $G_I$ of the parallel propeller-type G-quadruplex DNA ($PP_2$).

**Free Energy Calculations.** In order to have a better understanding of the selective association of TMPyP4 with each G-quadruplex DNA, we calculated the energies of the native G-quadruplex DNA along with its complex using MM_PBSA free energy analysis with a set of 100 snapshots obtained from the last 10 ns of the final production run of the MD simulations. It has been suggested by Jayaram et al.[80] and Štefl et al.[81] that the presence of the central $K^+$ ions is absolutely essential, since the thermodynamic calculations of the G-quadruplex DNA by MM_PBSA are not relevant when the $K^+$ ions are stripped off the central channel of the G-quartets. Hence, in all the simulation studies, we have placed two $K^+$ ions in the core of the G-quadruplex DNA.

For the analysis of the binding specificity of TMPyP4 to the various morphologies of the 22-mer G-quadruplexes, we determined the binding free energies of the TMPyP4−G-quadruplex complexes which are summarized in Table 4. Here the total gas phase energy ($\Delta E_{GAS}$), composed of electrostatic energy ($\Delta E_{ELEC}$) and van der Waals energy ($\Delta E_{VDW}$), shows a favorable contribution toward the binding of TMPyP4 to the G-quadruplex DNA. It is observed that the electrostatic contribution to solvation free energy shows a high positive


dx.doi.org/10.1021/jp505792z | J. Phys. Chem. B XXXX, XXX, XXX−XXX

Table 2. Hydrogen Bond Occurrence[a] during the Final Molecular Dynamics Simulation for 50 ns for the TMPyP4−G-Quadruplex DNA Complexes[b]

| | $PP_2$ | | $AB_2$ | | $MH_6$ | |
|---|---|---|---|---|---|---|
| | N2−H21···N7 | N1−H1···O6 | N2−H21···N7 | N1−H1···O6 | N2−H21···N7 | N1−H1···O6 |
| G2 | 98.6 | 98.7 | 99.5 | 99.6 | 99.4 | 99.8 |
| G3 | 99.8 | 96.8 | 99.4 | 84.5 | 99.3 | 96.0 |
| G4 | 99.4 | 99.9 | 99.7 | 100.0 | 99.6 | 99.7 |
| G8 | 97.7 | 98.3 | 96.6 | 99.8 | 98.8 | 99.8 |
| G9 | 99.7 | 97.0 | 99.3 | 93.5 | 99.8 | 98.3 |
| G10 | 98.8 | 99.9 | 99.5 | 99.6 | 99.1 | 99.8 |
| G14 | 99.0 | 98.6 | 99.8 | 100.0 | 99.1 | 99.8 |
| G15 | 99.7 | 97.0 | 99.8 | 91.9 | 99.9 | 95.2 |
| G16 | 98.8 | 99.9 | 98.9 | 99.9 | 100.0 | 99.9 |
| G20 | 99.7 | 99.4 | 99.8 | 99.9 | 99.9 | 99.8 |
| G21 | 99.9 | 97.2 | 95.1 | 81.2 | 99.9 | 97.9 |

[a]All the values shown are in percentages. [b]$PP_2$, $AB_2$, and $MH_6$ = most stable conformation of the complex between TMPyP4 and parallel propeller-type, antiparallel basket-type, and mixed hybrid-type G-quadruplex DNA, respectively. GX = guanine bases in the 22-mer sequence used, where X = residue number.

Table 3. Calculation of Solvent Accessible Surface Area and Related Data Obtained Due to the G-Quadruplex−TMPyP4 Complex Formation[a]

| | complex | | quadruplex | | TMPyP4 | | | |
|---|---|---|---|---|---|---|---|---|
| | SESA | SASA | SESA | SASA | SESA | SASA | ΔSESA | ΔSASA |
| $PP_2$ | 3602.28 | 4572.89 | 3414.54 | 4388.95 | 573.18 | 969.75 | −385.44 | −785.24 |
| $AB_2$ | 3153.51 | 4024.57 | 2900.94 | 3696.20 | 573.98 | 971.79 | −321.41 | −643.42 |
| $MH_6$ | 3399.85 | 4227.76 | 3171.80 | 3937.47 | 573.97 | 971.75 | −345.92 | −681.46 |

[a]$PP_2$, $AB_2$, and $MH_6$ = most stable conformation of the complex between TMPyP4 and parallel propeller-type, antiparallel basket-type, and mixed hybrid-type G-quadruplex DNA, respectively. SESA and SASA are the solvent excluded surface area and solvent accessible surface area, respectively. ΔSESA = SESA(complex) − [SESA(G-quadruplex) + SESA(TMPyP4)]. ΔSASA = SASA(complex) − [SASA(G-quadruplex) + SASA(TMPyP4)]. All the values are in $Å^2$.

Table 4. Contribution to the Binding Free Energies (kcal $mol^{-1}$) of the Different G-Quadruplex−TMPyP4 Complexes[a]

| | $\Delta E_{ELEC}$ | $\Delta E_{VDW}$ | $\Delta E_{INT}$ | $\Delta E_{GAS}$ | $\Delta G_{NP}$ | $\Delta G_{PB}$ | $\Delta G_{SOL}$ | $\Delta G$ |
|---|---|---|---|---|---|---|---|---|
| $PP_2$ | −1683 ± 35 | −54 ± 2 | 0.00 | −1737 ± 36 | −5.4 ± 0.2 | 1691 ± 35 | 1685 ± 35 | −51 ± 3 |
| $AB_2$ | −1596 ± 28 | −38 ± 3 | 0.00 | −1634 ± 30 | −4.2 ± 0.3 | 1596 ± 29 | 1592 ± 29 | −42 ± 3 |
| $MH_6$ | −1474 ± 28 | −38 ± 3 | 0.00 | −1512 ± 29 | −4.3 ± 0.3 | 1480 ± 29 | 1476 ± 29 | −36 ± 3 |

[a]$\Delta E_{ELEC}$ = electrostatic energy, $\Delta E_{VDW}$ = van der Waals contribution, $\Delta E_{INT}$ = the internal energy arising from bond angle and dihedral terms, $\Delta E_{GAS}$ = sum of $\Delta E_{ELEC}$, $\Delta E_{VDW}$ and $\Delta E_{INT}$ = total gas phase energy, $\Delta G_{NP}$ = nonpolar contribution to the solvation free energy, $\Delta G_{PB}$ = electrostatic contribution to the solvation free energy as obtained from the PB calculations, $\Delta G_{SOL}$ = sum of the polar and nonpolar contributions to the solvation free energy, $\Delta G = \Delta E_{GAS} + \Delta G_{SOL}$. Error bars denote standard deviation.

Table 5. Entropic Contributions (kcal $mol^{-1}$) of the Different G-Quadruplex DNA−TMPyP4 Complexes[a]

| | | complex | receptor | ligand | (complex−receptor−ligand) |
|---|---|---|---|---|---|
| $PP_2$ | translational | 15.7 ± 0.0 | 15.6 ± 0.0 | 13.5 ± 0.0 | −13.4 ± 0.0 |
| | rotational | 15.4 ± 0.0 | 15.3 ± 0.0 | 11.9 ± 0.0 | −11.9 ± 0.0 |
| | vibrational | 601 ± 2 | 550 ± 3 | 49.8 ± 0.1 | 1.2 ± 0.2 |
| | total | 632 ± 2 | 581 ± 3 | 75.2 ± 0.1 | −24 ± 2 |
| $AB_2$ | translational | 15.7 ± 0.0 | 15.6 ± 0.0 | 13.5 ± 0.0 | −13.4 ± 0.0 |
| | rotational | 15.2 ± 0.0 | 15.0 ± 0.0 | 11.9 ± 0.0 | −11.8 ± 0.0 |
| | vibrational | 592 ± 2 | 537 ± 2 | 49.4 ± 0.0 | 5 ± 1 |
| | total | 622 ± 2 | 568 ± 2 | 74.9 ± 0.0 | −20 ± 2 |
| $MH_6$ | translational | 15.7 ± 0.0 | 15.6 ± 0.0 | 13.5 ± 0.0 | −13.4 ± 0.0 |
| | rotational | 15.3 ± 0.0 | 15.1 ± 0.0 | 11.9 ± 0.0 | −11.8 ± 0.0 |
| | vibrational | 597 ± 1 | 543 ± 2 | 49.8 ± 0.1 | 4 ± 1 |
| | total | 628 ± 1 | 574 ± 2 | 75.3 ± 0.1 | −21 ± 1 |

[a]Translational, rotational, and vibrational components of the entropic contribution, $T\Delta S$, of the different TMPyP4−G-quadruplex DNA complexes. All entropic results have units of kcal $mol^{-1}$. Error bars denote standard deviation.

value for all three G-quadruplexes, while the nonpolar solvation free energy ($\Delta G_{NP}$) shows a stabilizing effect with a slightly better contribution from $PP_2$. From the binding free energy values obtained by the summation of $\Delta E_{GAS}$ and $\Delta G_{SOL}$, we


dx.doi.org/10.1021/jp505792z | J. Phys. Chem. B XXXX, XXX, XXX−XXX

observed that the $\Delta G$ value for $PP_2$ is far greater in magnitude than that for $AB_2$ and $MH_6$, thereby indicating that TMPyP4 is highly selective toward binding with parallel propeller-type G-quadruplex among all the G-quadruplexes under consideration.

The entropic contribution of the ligand (TMPyP4) due to its binding to various G-quadruplex DNA morphologies is almost the same. However, the loss of degrees of freedom of the DNA (translational, rotational, and vibrational) upon interaction with the drug cannot be neglected. Although the translational and rotational entropic contribution remains unchanged in all the G-quadruplex DNA structures upon binding to TMPyP4, there occurs a slight change in the vibrational entropic contribution. However, the total entropic costs due to TMPyP4−G-quadruplex DNA complex formation in all of the cases do not vary (−21 to −24 kcal $mol^{-1}$) (Table 5). Although the entropic contributions arising due to ligand−DNA binding are similar, it should be noted that the enthalpic contributions show different ligand−DNA binding affinities. In fact, the enthalpic contributions dominate over the entropic contributions and this results in the specificity of TMPyP4 binding to a particular G-quadruplex DNA conformation ($PP_2$) over its other polymorphs.

## CONCLUSIONS

The comparative study of TMPyP4 with an array of G-quadruplex DNA structures is essential in order to throw light on the plausible binding interaction of TMPyP4 with the human telomeric G-quadruplex DNA and get a clear indication about the efficiency of binding of TMPyP4 with the different kinds of human telomeric G-quadruplex DNA. Docking studies of TMPyP4 with different human G-quadruplex DNA revealed the most stable complex by considering all of the probable binding sites. Moreover, molecular dynamics simulation runs showed the stability of these docked complexes for a time duration of 50 ns. The hydrogen bonding of the guanine bases further substantiated this and also confirmed more conspicuous interaction of TMPyP4 with the parallel propeller-type DNA. Solvent accessible surface area along with the free energy of binding unanimously supported the better binding of TMPyP4 with the parallel propeller-type DNA. TMPyP4 thus has an inherent tendency to end-stack to the G-tetrads of the different G-quadruplex DNA due to the favorable $\pi-\pi$ interaction of the G-quartets with the core aromatic moieties of the ligand. This interaction is far greater in the case of parallel propeller-type G-quadruplex DNA in comparison to the other G-quadruplex morphologies where the interaction is mainly between the positively charged *N*-methylpyridinium side chains and negatively charged phosphate backbone in the grooves.

## ASSOCIATED CONTENT

### Supporting Information

Information on binding energy of "blind" docking, probable binding positions of G-quadruplex DNAs, and hydrogen bond occurrence of G-quadruplex DNAs. This material is available free of charge via the Internet at http://pubs.acs.org.

## AUTHOR INFORMATION

### Corresponding Author

*E-mail: sb@orgchem.iisc.ernet.in. Phone: (91)-80-22932664. Fax: (91)-80-22930529.

### Notes

The authors declare no competing financial interest.

## ACKNOWLEDGMENTS

We are thankful to Professor Prabal K. Maiti and Mr. D. K. Senthil Kumar for their help. All the calculations were performed at the Supercomputing cluster at the Molecular Biophysics Unit, Department of Organic Chemistry, and the Supercomputer Education and Research Centre, Indian Institute of Science, Bangalore, India. This work was supported by the funds from the J. C. Bose Fellowship grant of the DST (S.B.). A.A. thanks CSIR for a senior research fellowship.

## ABBREVIATIONS

PP, parallel propeller-type G-quadruplex DNA; AB, antiparallel basket-type G-quadruplex DNA; MH, mixed hybrid-type G-quadruplex DNA; TMPyP4, 5,10,15,20-tetra(*N*-methyl-4-pyridyl)porphine; B3LYP, Becke's three parameter hybrid functional using the Lee, Yang, and Parr correlation functional; $K^+$, potassium ion; MD, molecular dynamics; RMSD, root-mean-square deviation; GAFF, general AMBER force field; ns, nanosecond; ps, picosecond; fs, femtosecond; PME, particle mesh Ewald; MM_PBSA [molecular mechanics (MM), Poisson−Boltzmann (PB), surface area]; MSMS, Michel Sanner's molecular surface; VDW, van der Waals; SASA, solvent accessible surface area; SESA, solvent excluded surface area

## REFERENCES

(1) Wang, Y.; Patel, D. J. Solution Structure of the Tetrahymena Telomeric Repeat $d(T_2G_4)_4$ G-tetraplex. *Structure* **1994**, *2*, 1141−1156.

(2) Wellinger, R. J.; Sen, D. The DNA Structures at the Ends of Eukaryotic Chromosomes. *Eur. J. Cancer* **1997**, *33*, 735−749.

(3) Neidle, S.; Parkinson, G. Telomere Maintenance as a Target for Anticancer Drug Discovery. *Nat. Rev. Drug Discovery* **2002**, *1*, 383−393.

(4) Hurley, L. H. DNA and its Associated Processes as Targets for Cancer Therapy. *Nat. Rev. Cancer* **2002**, *2*, 188−200.

(5) Wright, W. E.; Tesmer, V. M.; Huffman, K. E.; Levene, S. D.; Shay, J. W. Normal Human Chromosomes Have Long G-rich Telomeric Overhangs at One End. *Genes Dev.* **1997**, *11*, 2801−2809.

(6) Greider, C. W.; Blackburn, E. H. Identification of a Specific Telomere Terminal Transferase Activity in Tetrahymena Extracts. *Cell* **1985**, *43*, 405−413.

(7) Kim, N. W.; Piatyszek, M. A.; Prowse, K. R.; Harley, C. B.; West, M. D.; Ho, P. L.; Coviello, G. M.; Wright, W. E.; Weinrich, S. L.; Shay, J. W. Specific Association of Human Telomerase Activity with Immortal Cells and Cancer. *Science* **1994**, *266*, 2011−2015.

(8) Zahler, A. M.; Williamson, J. R.; Cech, T. R.; Prescott, D. M. Inhibition of Telomerase by G-quartet DNA Structures. *Nature* **1991**, *350*, 718−720.

(9) Zaug, A. J.; Podell, E. R.; Cech, T. R. Human POT1 Disrupts Telomeric G-quadruplexes Allowing Telomerase Extension *in vitro*. *Proc. Natl. Acad. Sci. U.S.A.* **2005**, *102*, 10864−10869.

(10) Gellert, M.; Lipsett, M. N.; Davies, D. R. Helix Formation by Guanylic Acid. *Proc. Natl. Acad. Sci. U.S.A.* **1962**, *48*, 2013−2018.

(11) Guschlbauer, W.; Chantot, J. F.; Theile, D. Four-Stranded Nucleic Acid Structures 25 Years Later: From Guanosine Gels to Telomer DNA. *J. Biomol. Struct. Dyn.* **1990**, *8*, 491−511.

(12) Mergny, J. L.; Riou, J. F.; Mailliet, P.; Teulade-Fichou, M. P.; Gilson, E. Natural and Pharmacological Regulation of Telomerase. *Nucleic Acids Res.* **2002**, *30*, 839−865.

(13) Gomez, D.; O'Donohue, M. F.; Wenner, T.; Douarre, C.; Macadré, J.; Koebel, P.; Giraud-Panis, M. J.; Kaplan, H.; Kolkes, A.; Shin-ya, K.; et al. The G-quadruplex Ligand Telomestatin Inhibits POT1 Binding to Telomeric Sequences *In vitro* and Induces GFP-POT1 Dissociation from Telomeres in Human Cells. *Cancer Res.* **2006**, *66*, 6908−6912.

(14) Jain, A. K.; Bhattacharya, S. Interaction of G-Quadruplexes with Nonintercalating Duplex-DNA Minor Groove Binding Ligands. *Bioconjugate Chem.* **2011**, *22*, 2355−2368.
(15) Paul, A.; Bhattacharya, S. Chemistry and Biology of DNA-Binding Small Molecules. *Curr. Sci.* **2012**, *102*, 212−231.
(16) Maji, B.; Bhattacharya, S. Advances in the Molecular Design of Potential Anticancer Agents *via* Targeting of Human Telomeric DNA. *Chem. Commun.* **2014**, *50*, 6422−6438.
(17) Ali, A.; Bhattacharya, S. DNA Binders in Clinical Trials and Chemotherapy. *Bioorg. Med. Chem.* **2014**, *22*, 4506−4521.
(18) Fry, M.; Loeb, L. A. The Fragile X Syndrome $d(CGG)_n$ Nucleotide Repeats Form a Stable Tetrahelical Structure. *Proc. Natl. Acad. Sci. U.S.A.* **1994**, *91*, 4950−4954.
(19) Nadel, Y.; Weisman-Shomer, P.; Fry, M. The Fragile X Syndrome Single Strand $d(CGG)_n$ Nucleotide Repeats Readily Fold Back to Form Unimolecular Hairpin Structures. *J. Biol. Chem.* **1995**, *270*, 28970−28977.
(20) Hammond-Kosack, M. C. U.; Kilpatrick, M. W.; Docherty, K. Analysis of DNA Structure in the Human Insulin Gene-linked Polymorphic Region *in vivo*. *J. Mol. Endocrinol.* **1992**, *9*, 221−225.
(21) Sundquist, W. I.; Heaphy, S. Evidence for Interstrand Quadruplex Formation in the Dimerization of Human Immunodeficiency Virus 1 Genomic RNA. *Proc. Natl. Acad. Sci. U.S.A.* **1993**, *90*, 3393−3397.
(22) Simonsson, T.; Pecinka, P.; Kubista, M. DNA Tetraplex Formation in the Control Region of *c-myc*. *Nucleic Acids Res.* **1998**, *26*, 1167−1172.
(23) Read, M. A.; Neidle, S. Structural Characterization of a Guanine-Quadruplex Ligand Complex. *Biochemistry* **2000**, *39*, 13422−13432.
(24) Kim, M. Y.; Vankayalapati, H.; Shin-Ya, K.; Wierzba, K.; Hurley, L. H. Telomestatin, a Potent Telomerase Inhibitor That Interacts Quite Specifically with the Human Telomeric Intramolecular G-Quadruplex. *J. Am. Chem. Soc.* **2002**, *124*, 2098−2099.
(25) Perry, P. J.; Read, M. A.; Davies, R. T.; Gowan, S. M.; Reszka, A. P.; Wood, A. A.; Kelland, L. R.; Neidle, S. 2,7-Disubstituted Amidofluorenone Derivatives as Inhibitors of Human Telomerase. *J. Med. Chem.* **1999**, *42*, 2679−2684.
(26) Fedoroff, O. Y.; Salazar, M.; Han, H.; Chemeris, V. V.; Kerwin, S. M.; Hurley, L. H. NMR-Based Model of a Telomerase-Inhibiting Compound Bound to G-Quadruplex DNA. *Biochemistry* **1998**, *37*, 12367−12374.
(27) Han, H.; Cliff, C. L.; Hurley, L. H. Accelerated Assembly of G-Quadruplex Structures by a Small Molecule. *Biochemistry* **1999**, *38*, 6981−6986.
(28) Martins, C.; Gunaratnam, M.; Stuart, J.; Makwana, V.; Greciano, O.; Reszka, A. P.; Kelland, L. R.; Neidle, S. Structure-Based Design of Benzylamino-Acridine Compounds as G-quadruplex DNA Telomere Targeting Agents. *Bioorg. Med. Chem. Lett.* **2007**, *17*, 2293−2298.
(29) Moore, M. J. B.; Schultes, C. M.; Cuesta, J.; Cuenca, F.; Gunaratnam, M.; Tanious, F. A.; Wilson, W. D.; Neidle, S. Trisubstituted Acridines as G-quadruplex Telomere Targeting Agents. Effects of Extensions of the 3,6- and 9-Side Chains on Quadruplex Binding, Telomerase Activity, and Cell Proliferation. *J. Med. Chem.* **2006**, *49*, 582−599.
(30) Paul, A.; Jain, A. K.; Misra, S. K.; Maji, B.; Muniyappa, K.; Bhattacharya, S. Binding of Gemini Bisbenzimidazole Drugs with Human Telomeric G-Quadruplex Dimers: Effect of the Spacer in the Design of Potent Telomerase Inhibitors. *PLoS One* **2012**, *7*, e39467.
(31) Jain, A. K.; Paul, A.; Maji, B.; Muniyappa, K.; Bhattacharya, S. Dimeric 1,3-phenylene-bis(piperazinyl benzimidazole)s: Synthesis and Structure-Activity Investigations on their Binding with Human Telomeric G-Quadruplex DNA and Telomerase Inhibition Properties. *J. Med. Chem.* **2012**, *55*, 2981−2993.
(32) Paul, A.; Maji, B.; Misra, S. K.; Jain, A. K.; Muniyappa, K.; Bhattacharya, S. Stabilization and Structural Alteration of the G-Quadruplex DNA Made from the Human Telomeric Repeat Mediated by Tröger's Base Based Novel Benzimidazole Derivatives. *J. Med. Chem.* **2012**, *55*, 7460−7471.
(33) Bhattacharya, S.; Chaudhuri, P.; Jain, A. K.; Paul, A. Symmetrical Bisbenzimidazoles with Benzenediyl Spacer: The Role of the Shape of the Ligand on the Stabilization and Structural Alterations in Telomeric G-Quadruplex DNA and Telomerase Inhibition. *Bioconjugate Chem.* **2010**, *21*, 1148−1159.
(34) Jain, A. K.; Reddy, V. V.; Paul, A.; Muniyappa, K.; Bhattacharya, S. Synthesis and Evaluation of a Novel Class of G-Quadruplex-Stabilizing Small Molecules Based on the 1,3-Phenylene-Bis-(piperazinyl benzimidazole) System. *Biochemistry* **2009**, *48*, 10693−10704.
(35) Maji, B.; Bhattacharya, S. Molecular Design of Synthetic Benzimidazoles for the Switchover of the Duplex to G-quadruplex DNA Recognition. *Chimia* **2013**, *67*, 39−43.
(36) Wei, C.; Jia, G.; Yuan, J.; Feng, Z.; Li, C. A Spectroscopic Study on the Interactions of Porphyrin with G-quadruplex DNAs. *Biochemistry* **2006**, *45*, 6681−6691.
(37) Freyer, M. W.; Buscaglia, R.; Kaplan, K.; Cashman, D.; Hurley, L. H.; Lewis, E. A. Biophysical Studies of the c-MYC NHE III1 Promoter: Model Quadruplex Interactions with a Cationic Porphyrin. *Biophys. J.* **2007**, *92*, 2007−2015.
(38) Izbicka, E.; Wheelhouse, R. T.; Raymond, E.; Davidson, K. K.; Lawrence, R. A.; Sun, D.; Windle, B. E.; Hurley, L. H.; Von Hoff, D. D. Effects of Cationic Porphyrins as G-Quadruplex Interactive Agents in Human Tumor Cells. *Cancer Res.* **1999**, *59*, 639−644.
(39) Dixon, I. M.; Lopez, F.; Estève, J. P.; Tejera, A. M.; Blasco, M. A.; Pratviel, G.; Meunier, B. Porphyrin Derivatives for Telomere Binding and Telomerase Inhibition. *ChemBioChem* **2005**, *6*, 123−132.
(40) Shi, D. F.; Wheelhouse, R. T.; Sun, D.; Hurley, L. H. Quadruplex-Interactive Agents as Telomerase Inhibitors: Synthesis of Porphyrins and Structure-Activity Relationship for the Inhibition of Telomerase. *J. Med. Chem.* **2001**, *44*, 4509−4523.
(41) Martino, L.; Pagano, B.; Fotticchia, I.; Neidle, S.; Giancola, C. Shedding Light on the Interaction between TMPyP4 and Human Telomeric Quadruplexes. *J. Phys. Chem. B* **2009**, *113*, 14779−14786.
(42) Zhang, H. J.; Wang, X. F.; Wang, P.; Ai, X. C.; Zhang, J. P. Spectroscopic Study on the Binding of a Cationic Porphyrin to DNA G-quadruplex Under Different $K^+$ Concentrations. *Photochem. Photobiol. Sci.* **2008**, *7*, 948−955.
(43) Nagesh, N.; Buscaglia, R.; Dettler, J. M.; Lewis, E. A. Studies on the Site and Mode of TMPyP4 Interactions with Bcl-2 Promoter Sequence G-Quadruplexes. *Biophys. J.* **2010**, *98*, 2628−2633.
(44) Han, H.; Langley, D. R.; Rangan, A.; Hurley, L. H. Selective Interactions of Cationic Porphyrins with G-Quadruplex Structures. *J. Am. Chem. Soc.* **2001**, *123*, 8902−8913.
(45) Anantha, N. V.; Azam, M.; Sheardy, R. D. Porphyrin Binding to Quadruplexed $T_4G_4$. *Biochemistry* **1998**, *37*, 2709−2714.
(46) Wheelhouse, R. T.; Sun, D.; Han, H.; Han, F. X.; Hurley, L. H. Cationic Porphyrins as Telomerase Inhibitors: The Interaction of Tetra-(*N*-methyl-4-pyridyl)porphine with Quadruplex DNA. *J. Am. Chem. Soc.* **1998**, *120*, 3261−3262.
(47) Parkinson, G. N.; Lee, M. P.; Neidle, S. Crystal Structure of Parallel Quadruplexes from Human Telomeric DNA. *Nature* **2002**, *417*, 876−880.
(48) Wang, Y.; Patel, D. J. Solution Structure of the Human Telomeric Repeat $d[AG_3(T_2AG_3)_3]$ G-tetraplex. *Structure* **1993**, *1*, 263−282.
(49) Dai, J.; Punchihewa, C.; Ambrus, A.; Chen, D.; Jones, R. A.; Yang, D. Structure of the Intramolecular Human Telomeric G-quadruplex in Potassium Solution: A Novel Adenine Triple Formation. *Nucleic Acids Res.* **2007**, *35*, 2440−2450.
(50) Frisch, M. J.; Trucks, G. W.; Schlegel, H. B.; Scuseria, G. E.; Robb, M. A.; Cheeseman, J. R.; Montgomery, J. A., Jr.; Vreven, T.; Kudin, K. N.; Burant, J. C.; et al. *Gaussian 03*; Gaussian, Inc.: Wallingford, CT, 2004.
(51) Case, D. A.; Darden, T. A.; Cheatham, T. E., III; Simmerling, C. L.; Wang, J.; Duke, R. E.; Luo, R.; Merz, K. M.; Pearlman, D. A.; Crowley, M.; et al. *Amber 9*; University of California: San Francisco, CA, 2006.

(52) Wang, J.; Wolf, R. M.; Caldwell, J. W.; Kollman, P. A.; Case, D. A. Development and Testing of a General Amber Force Field. *J. Comput. Chem.* **2004**, *25*, 1157−1174.
(53) Morris, G. M.; Goodsell, D. S.; Halliday, R. S.; Huey, R.; Hart, W. E.; Belew, R. K.; Olson, A. J. Automated Docking Using a Lamarckian Genetic Algorithm and an Empirical Binding Free Energy Function. *J. Comput. Chem.* **1998**, *19*, 1639−1662.
(54) Huey, R.; Morris, G. M.; Olson, A. J.; Goodsell, D. S. A Semiempirical Free Energy Force Field with Charge-Based Desolvation. *J. Comput. Chem.* **2007**, *28*, 1145−1152.
(55) Sanner, M. F. Python: A Programming Language for Software Integration and Development. *J. Mol. Graphics Modell.* **1999**, *17*, 57−61.
(56) Solis, F. J.; Wets, J.-B. Minimization by Random Search Techniques. *Math. Oper. Res.* **1981**, *6*, 19−30.
(57) Pérez, A.; Luque, F. J.; Orozco, M. Frontiers in Molecular Dynamics Simulations of DNA. *Acc. Chem. Res.* **2012**, *45*, 196−205.
(58) Norberg, J.; Nilsson, L. Molecular Dynamics Applied to Nucleic Acids. *Acc. Chem. Res.* **2002**, *35*, 465−472.
(59) Cornell, W. D.; Cieplak, P.; Bayly, C. I.; Gould, I. R.; Merz, K. M.; Ferguson, D. M.; Spellmeyer, D. C.; Fox, T.; Caldwell, J. W.; Kollman, P. A. A Second Generation Force Field for the Simulation of Proteins, Nucleic Acids, and Organic Molecules. *J. Am. Chem. Soc.* **1995**, *117*, 5179−5197.
(60) Cheatham, T. E., 3rd; Cieplak, P.; Kollman, P. A. A Modified Version of the Cornell *et al*. Force Field with Improved Sugar Pucker Phases and Helical Repeat. *J. Biomol. Struct. Dyn.* **1999**, *16*, 845−862.
(61) Pérez, A.; Marchán, I.; Svozil, D.; Sponer, J.; Cheatham, T. E., 3rd.; Laughton, C. A.; Orozco, M. Refinement of the AMBER Force Field for Nucleic Acids: Improving the Description of Alpha/Gamma Conformers. *Biophys. J.* **2007**, *92*, 3817−3829.
(62) Di Leva, F. S.; Novellino, E.; Cavalli, A.; Parrinello, M.; Limongelli, V. Mechanistic Insight into Ligand Binding to G-quadruplex DNA. *Nucleic Acids Res.* **2014**, *42*, 5447−5455.
(63) Rahman, K. M.; Corcoran, D. B.; Bui, T. T. T.; Jackson, P. J. M.; Thurston, D. E. Pyrrolobenzodiazepines (PBDs) Do Not Bind to DNA G-Quadruplexes. *PLoS One* **2014**, *9*, e105021.
(64) Novotný, J.; Yurenko, Y. P.; Kulhánek, P.; Marek, R. Tailoring the Properties of Quadruplex Nucleobases for Biological and Nanomaterial Applications. *Phys. Chem. Chem. Phys.* **2014**, *16*, 15241−15248.
(65) *The PyMOL Molecular Graphics System*, version 0.99rc6; Schrödinger, LLC.
(66) Humphrey, W.; Dalke, A.; Schulten, K. VMD: Visual Molecular Dynamics. *J. Mol. Graphics* **1996**, *14*, 33−38.
(67) Luo, R.; David, L.; Gilson, M. K. Accelerated Poisson−Boltzmann Calculations for Static and Dynamic Systems. *J. Comput. Chem.* **2002**, *23*, 1244−1253.
(68) Pauling, L. The Sizes of Ions and the Structure of Ionic Crystals. *J. Am. Chem. Soc.* **1927**, *49*, 765−790.
(69) Sitkoff, D.; Sharp, K. A.; Honig, B. Correlating Solvation Free Energies and Surface Tensions of Hydrocarbon Solutes. *Biophys. Chem.* **1994**, *51*, 397−409.
(70) Agrawal, S.; Ojha, R. P.; Maiti, S. Energetics of the Human Tel-22 Quadruplex-Telomestatin Interaction: A Molecular Dynamics Study. *J. Phys. Chem. B* **2008**, *112*, 6828−6836.
(71) Sanner, M. F.; Olson, A. J.; Spehner, J. C. Reduced Surface: An Efficient Way to Compute Molecular Surfaces. *Biopolymers* **1996**, *38*, 305−320.
(72) Wei, C.; Jia, G.; Zhou, J.; Han, G.; Li, C. Evidence for the Binding Mode of Porphyrins to G-quadruplex DNA. *Phys. Chem. Chem. Phys.* **2009**, *11*, 4025−4032.
(73) Islam, B.; Sgobba, M.; Laughton, C.; Orozco, M.; Sponer, J.; Neidle, S.; Haider, S. Conformational Dynamics of the Human Propeller Telomeric DNA Quadruplex on a Microsecond Time Scale. *Nucleic Acids Res.* **2013**, *41*, 2723−2735.
(74) Haq, I.; Trent, J. O.; Chowdhry, B. Z.; Jenkins, T. C. Intercalative G-Tetraplex Stabilization of Telomeric DNA by a Cationic Porphyrin. *J. Am. Chem. Soc.* **1999**, *121*, 1768−1779.
(75) Chowdhury, S.; Bansal, M. Effect of Coordinated Ions on Structure and Flexibility of Parallel G-quadruplexes: A Molecular Dynamics Study. *J. Biomol. Struct. Dyn.* **2000**, *17*, 11−28.
(76) Chowdhury, S.; Bansal, M. A Nanosecond Molecular Dynamics Study of Antiparallel $d(G)_7$ Quadruplex Structures: Effect of the Coordinated Cations. *J. Biomol. Struct. Dyn.* **2001**, *18*, 647−669.
(77) Chowdhury, S.; Bansal, M. G-Quadruplex Structure Can Be Stable with Only Some Coordination Sites Being Occupied by Cations: A Six-Nanosecond Molecular Dynamics Study. *J. Phys. Chem. B* **2001**, *105*, 7572−7578.
(78) Neidle, S.; Read, M. A. G-Quadruplexes as Therapeutic Targets. *Biopolymers* **2001**, *56*, 195−208.
(79) Blackburn, E. H. Telomeres: No End in Sight. *Cell* **1994**, *77*, 621−623.
(80) Jayaram, B.; Sprous, D.; Young, M. A.; Beveridge, D. L. Free Energy Analysis of the Conformational Preferences of A and B Forms of DNA in Solution. *J. Am. Chem. Soc.* **1998**, *120*, 10629−10633.
(81) Štefl, R.; Cheatham, T. E., III; Špačková, N.; Fadrná, E.; Berger, I.; Koča, J.; Šponer, J. Formation Pathways of a Guanine-Quadruplex DNA Revealed by Molecular Dynamics and Thermodynamic Analysis of the Substates. *Biophys. J.* **2003**, *85*, 1787−1804.